Scanning Tunneling Microscopy of Diamond Coated Surfaces

Bachelor thesis

Walter Lukesch, 0230661

01.02.2010

Ao.Univ.-Prof. Dipl.-Ing. Dr.techn. tit.Univ.-Prof. Manfred Leisch

0. Abstract

The aim of this bachelor thesis is to perform a surface characterization of four diamond coated samples and to compare the results. Three of the samples have a boron doped layer with a thickness of 100, 200 and 500nm. The fourth has a 500nm thick undoped diamond layer. All of these scans are made with a scanning tunneling microscope. Accompanying to the images a height analysis and spectroscopic analysis are performed.

1. Introduction

1.1. The Tunnel Effect

The tunnel effect is a quantum mechanical effect discovered by Robert Williams Wood in the late 1890s. It is the explanation why the classically not possible working principle of scanning tunneling microscopy works. Because in the point of view of classic physics a particle cannot get through a potential, with a higher energy than the particle itself and has to be reflected. Demonstratively it can be compared to a ball which wasn't thrown with enough power to get over a wall and then simply bounces off the wall. But quantum mechanics mathematically shows in theory and in a lot of applications and experiments that the particle has a not disappearing probability to be found on the other side of the energy barrier.

To calculate the probability of the spatial density the Schrödinger equation has to be solved:

$$\left(-\frac{\hbar^2}{2m}\nabla^2 + V(\vec{x})\right)\psi(\vec{x}) = E\psi(\vec{x})$$

$$\Psi(\vec{x},t) = e^{-\frac{i}{\hbar}Et}\psi(\vec{x})$$

Ψ is the wave function; ħ the Plank constant divided by 2*π; E the energy and eigenfunction of the Hamiltonian function; m the mass; $V(\vec{x})$ the potential of the particle

The solution of the Schrödinger equation can be obtained using some boundary conditions, namely continuity and norm conditions of the wave function. As a result one gets three equivalent equations which are useful for different preconditions: (solution in one dimension)

$$\psi(x) = a_1 e^{\kappa x} + b_1 e^{-\kappa x} = a_2 e^{ikx} + b_2 e^{-ikx} = a_3 \cos(kx) + b_3 \sin(kx)$$

Where $k^2 = -\kappa^2 = \frac{2m}{\hbar}(E - V)$

For E < V the function shows an exponential behaviour and the first solution is an implementable equation. If E > V, the second solution works better, because k becomes a real number. In this case the wave function shows an oscillating behaviour.
As already described earlier, the tunnel effect is an effect which deals with a free particle advancing a barrier of high potential. For the calculation the hole space is mathematically separated into three different parts: the spaces on the left and the right hand side of the barrier and the barrier itself. Outside the barrier the particle shows an oscillating and within an exponential decreasing behaviour as shown in figure 1.

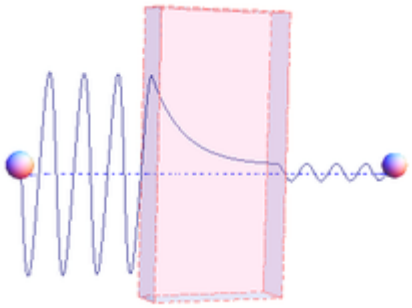

figure 1: The tunnel effect
(http://en.wikipedia.org/wiki/Quantum_tunnelling)

In the case of a very high and broad barrier it is useful to look at the transmission coefficient. This is the probability to get through the barrier. Of course, the sum of reflection and transmission is one, which means that no particle simply disappears. The transmission coefficient is:

$$T = \frac{\rho^2}{(1+\rho^2)\sinh^2(\kappa L) + 4\rho^2}$$

Where $\rho = \frac{\kappa}{k}$ and L the length of the barrier

Looking again at the special case of a very high and broad barrier the sinh simplifies to:

$$\sinh^2(\kappa L) \cong \frac{e^{2\kappa L}}{4} \gg 1$$

Which leads to:

$$T \cong \frac{4\rho^2}{(1+\rho^2)^2} 4e^{-2\kappa L}$$

In words, the transmission coefficient decreases exponentially with the barrier height and width (because of the factor $e^{-2\kappa L}$). Only in the case of an infinite high or broad barrier the probability of transmission turns into zero. This is why the scanning tunneling microscope actually works.

With these equations the tunnel current can be calculated. The current has an exponential dependence to the tip- surface distance:

$$I \propto e^{-A\sqrt{\phi}s}$$

Where I is the current, ϕ the mean local tunneling barrier height, s the distance and $A \approx 1\text{Å}^{-1} eV^{-\frac{1}{2}}$

One can see that this is a very convenient solution for the scanning tunneling microscope (STM) setup. Because of the fact that the current is exponentially dependent on the distance between tip and the surface very small distance variations result in relatively large current variations which is obviously very useful for the topography measurements. [1] [2]

1.2. The Scanning Tunneling Microscope

After the invention of scanning tunneling microscopy (STM) in 1981 by G. Binnig and H. Rohrer at the IBM Zürich Research Laboratory the field of STM grew rapidly and became a valuable, nearly indispensable surface analysis technique. Reasons for that are obviously the relative simplicity of the setup and the analysis of the received data. The idea of STM is to bring a conducting metal tip within a close distance to the sample. After the approximation the tip is directed above the surface and with an applied voltage a tunneling current can flow between the electrodes (as will be specified later). Another application of the STM is not only to scan the topography of the sample but to take also spectroscopic measurements. [3] [4]

1.2.1. Working Principles and Setup

The basic concept of the scanning tunneling microscopy is moving a sharp metallic needle over a surface and to measuring a tunnel current and gap voltage simultaneously.

The basic setup is shown in figure 2

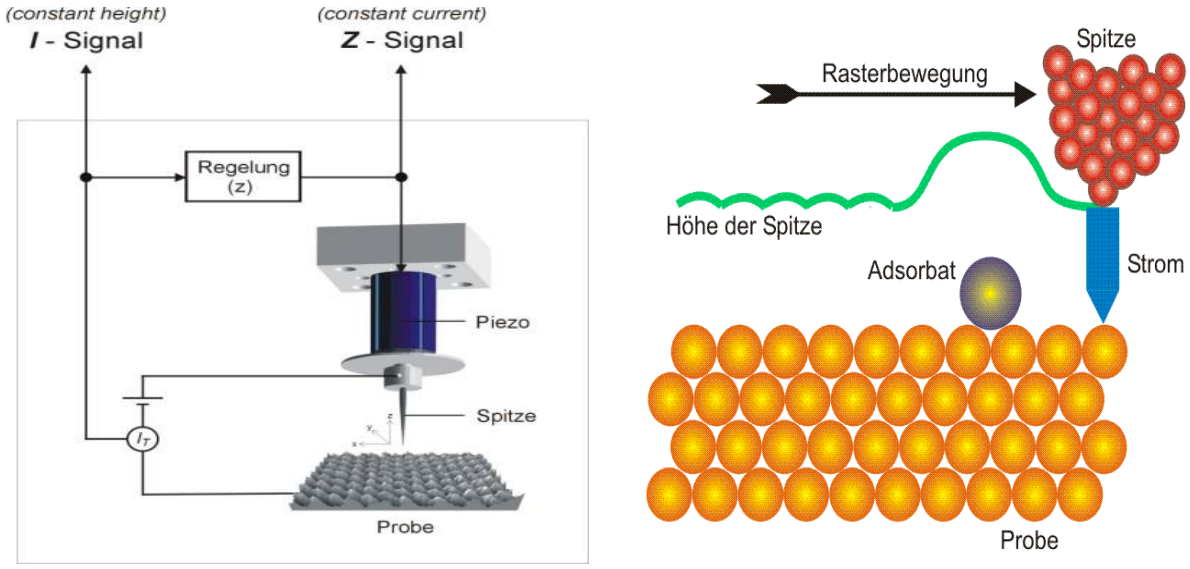

figure 2: setup of a STM and image formation
(http://de.wikipedia.org/wiki/Rastertunnelmikroskop)
(http://www.physnet.uni-hamburg.de/iap/group_g/F_Praktikum/Rastertunnelmikroskopie/stm1.gif)

The tip is mounted on a piezoelectric drive with which the tip can be adjusted precisely above the sample. There are two main modes in which the microscope can operate: The constant height and the constant current mode. In the constant height mode the tip is moved rapidly above the sample and variations of the tunnel current are recorded as a function of the position. The advantages of this mode are a relatively high scanvelocity and the avoidance of image distortions caused by the piezoelectric drive or thermal drifts. On the other hand, the constant height mode can only be used with very plane specimen, otherwise the tip could crash into protrusions. For surfaces which are not plane the constant current mode is more useful. In this mode the tip is adjusted above the sample with the piezoelectric drive that way that the tunnel current is held constant while moving. The voltage applied to the drive is proportional to the height of the tip, the measurement of this voltage as function of the position provides the information of the surface. A disadvantage of this operating mode is that the piezoelectric drive has a hysteresis which can distort the obtained information. Compared to the constant height mode the tip cannot be scanned that fast over the surface, due to the fact that the drive needs some time to place the tip in the right position. Another mode would be the differential microscopy, in which the tip is made to vibrate parallel to the surface. To obtain information about the electronic states of the material the spectroscopy mode is used. The gap voltage dependence of the tunnel current is observed in order to obtain information about the unoccupied, respectively occupied, states of the sample.

The measurements are usually made at ultrahigh vacuum conditions, but would generally be also possible in air. In ultrahigh vacuum the surface of the sample is much cleaner and there are not so many atoms or molecules which exert bad influences on the measurements.

In order to receive good results it is important to have a precisely shaped tip. The tips can be shaped by mechanical grinding or chemical edging. For general purposes tips made of tungsten are used very often. The aim is to create a one atom tip, because the further most atom has the greatest influence on the measurements. The exponential relation of the distance between the tip and the surface and the tunnel current is shown in the chapter 1.1.

In addition, it is necessary to mention that not the real topography is shown in the images made. As it is shown in figure 1 on the right side, the tip does not scan the real geometric structure of the surface, but in fact the map of constant density of states. The consequence is that an impurity on the surface or within the crystal structure can cause considerable aberrations in the taken images. But this circumstance is not that severe and STM is still the most accurate and detailed method for high resolution microscopy. [3] [4]

1.3. Comparative Analysis of Graphite and Diamond Structures

Graphite and diamond are both different structures of the same element, carbon. Although they are built up by the same element, they have very different properties. This is a result of their different atomic structure.

Diamond crystallizes in a face centered cubic (fcc) arrangement, which in fact can also be seen as two fcc lattices. One of those lattices is positioned inside the other one shifted by a quarter of the lattice vector along the direction of the diagonal. The four closest neighbours of a carbon atom surround the central atom in a tetrahedron arrangement. This is because of the hybridization of the highest orbital of the carbon atom ($1s^2 2p^2 2s^2$) into a sp^3 orbital. So the atoms arrange with the largest possible angle they are able to, which is 109,5 degrees.

Graphite, on the other hand, crystallizes in flat layers with sp^2 hybridized carbon atoms on the edges of a hexagon structure. In a graphite sample these layers are then arranged parallel above each other.

These crystal structures cause a lot of different material properties: The most remarkable is perhaps the appearance, and also hardness and conductivity differ much. The transparent diamond is the hardest natural material known, while graphite is a very soft mineral. Graphite has (in direction of the layers) a nearly metallic conductivity, while diamond is in principle conductive and shows a semiconductor characteristic. The following figures show the different lattices of the two materials. [5]

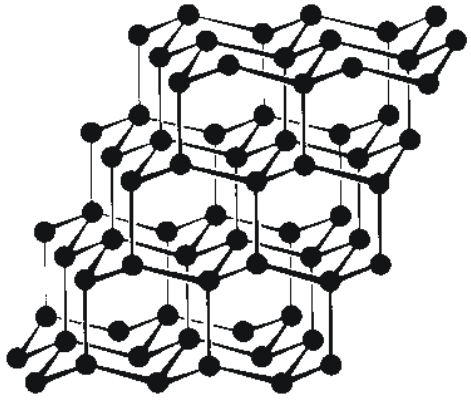

figure 3: Atomic structure of diamond (http://www.guidobauersachs.de/anorg/diamant.gif)

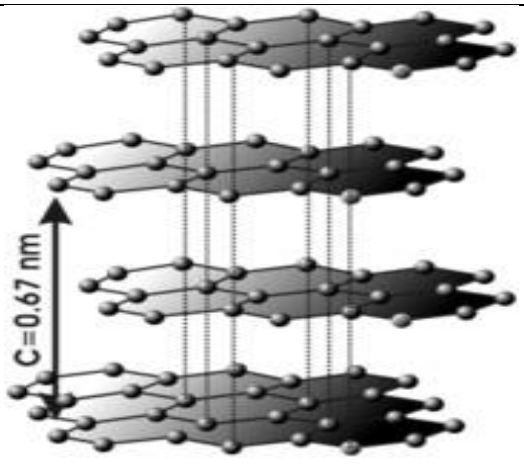

figure 4: Atomic structure of graphite (http://www.mineralienwissen.de/mineralien/graphit-struktur.jpg)

2. Experiment

2.1. Equipment List and Setup

All measurements were taken with the same devices which mainly are:

- An ultra high vacuum scanning tunneling microscope with a working pressure of $p < 5 * 10^{-9} mbar$ contains a sample holder and the scanning tunneling microscope itself with a tungsten tip. There are several other devices attached to the microscope equipment, e.g. a sputtering gun and a heating wire. Above the sample holder there is a video camera mounted, which is connected to a monitor. With the help of this equipment one can easily control the approach of the tip towards the specimen.
- The microscope control unit was a STM CONTROL UNIT from Omicron Vakuumphysik GmbH
- For the input and the calculation, a personal computer was used. For the input a STM-software and for further processing several image processing programs were used, by name: WSxM 5.0 Develop 1.2 by nanotech and ACD SEE photo software

To start the measurements at first one has to direct the tungsten tip in close range to the sample surface. The tip can be moved with an electronic drive with adjustable velocity closer to the sample. But the approach should be stopped early enough to avoid crashes into the surface which would cause irreparable damages to the tip and of course also to the sample itself. The approach is visually controlled over a monitor which receives its pictures from the attached camera. For the last micro-, respectively, nanometers the control unit has an automatic approach mode. An oscilloscope is used to control the stability of the tunneling contact between the tip and the probe.

Before the approach it is necessary to set a gap voltage and current on the control unit: the value in all of these measurements was 3V and 0,1nA. Furthermore the position of the frame can be set by adjusting the tip in x and y direction (with an overall range of 2000nm in each direction).
The last step before starting the measurements is to set the parameters on the computer. The necessary inputs are:

- The size of the imaged area in Angstrom
- The stepsize (meaning the number of points per line and the number of lines itself)
- The time used for each single step in milliseconds

For spectrographic measurements also:

- The type of spectroscopy (U/I)
- The step size, the number of steps and the range for the gapvoltage

These data is stored in an image parameter file.
In order to test the system, to check the piezoconstants and to verify the different parameters of the microscope, a plane sample with known properties was used: a graphite sample.

2.2. Graphite Sample

The graphite sample has a very plane surface structure and therefore it is a well suited object for testing the system. This was done by varying the acquisition parameters like frame- and step- size, or the time constants, and to check the effects in order to receive the best results.

The image processing programs have a few tools which help to create ameliorated micrographs. There are a lot of possibilities to display the recorded data, e.g. a two- or three dimensional image, but also an image of the derived data can be processed. It depends on the surface structure and the favoured result, which type of image processing is to be used.

The following images show a 50 x 50Å area of the graphite surface. In figure 5 one can see a raw micrograph of the sample. Figure 6 on the other hand shows a smoothed micrograph of the same data. For smoothing a Gauss- filter was applied which uses the next 5 neighbours to calculate the pixels. The figures 7 and 8 show the corresponding 3 dimensional plots to figures 5 and 6. The surfacestructure of the graphite sample is clearly visible in the three dimensional images. Compared to the two- dimensional diagram the three dimensional is much more significant and descriptive.

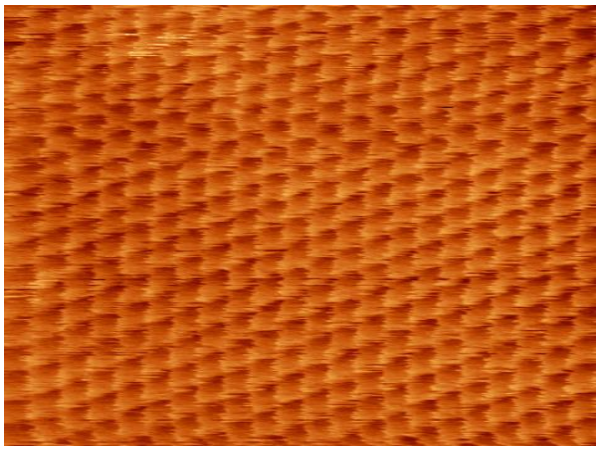

figure 5: two dimensional raw image of graphite (50x 50Å; 3V; 0,1nA; 1540µs at 1600 steps)

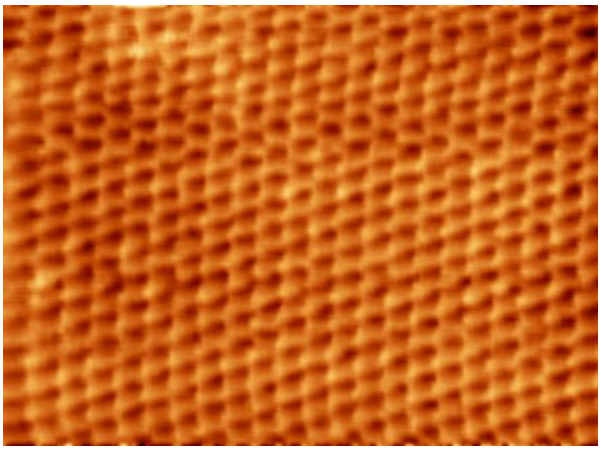

figure 6: two dimensional smoothed image of graphite (50x 50Å; 3V; 0,1nA; 1540µs at 1600 steps)

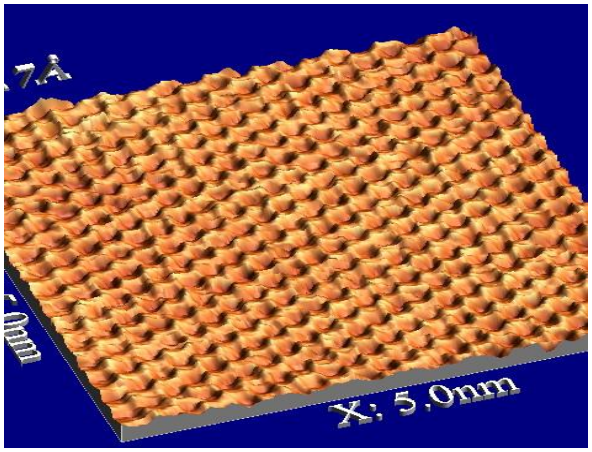

figure 7: three dimensional image of figure 5 (50x 50Å; 3V; 0,1nA; 1540µs at 1600 steps)

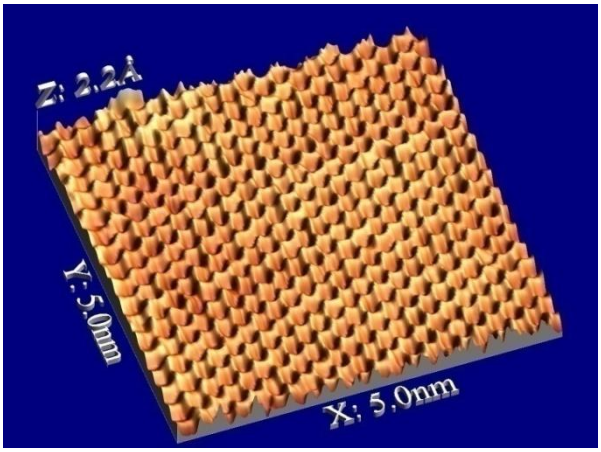

figure 8: three dimensional image of figure 6 (50x 50Å; 3V; 0,1nA; 1540µs at 1600 steps)

As can be seen in figure 5 high resolution images show lines in the micrograph. The lines derive from artifacts of adsorbates and contaminations on the sample surface. It depends on the sample material, of course the coverage of the surface and on the measurement settings. The faster the measurements are taken and the less measurement points are used the more aberrations will occur and the more diffused the image will be. Repeated measurements can minimize this effect and lead to better results because contaminations on the sample can get swept out of the measured area during the process.
Depending on the samplematerial, especially the bond type, the hybridization and corrugation, the quality of the received data differ can a lot.

In figure 9 a typical I(U) spectroscopy is plotted. The measurement was taken on the same area which is displayed above in the figures 5 to 8. The figure shows two curves in order to show the difference between a high point (red points) and a hollow (black squares).

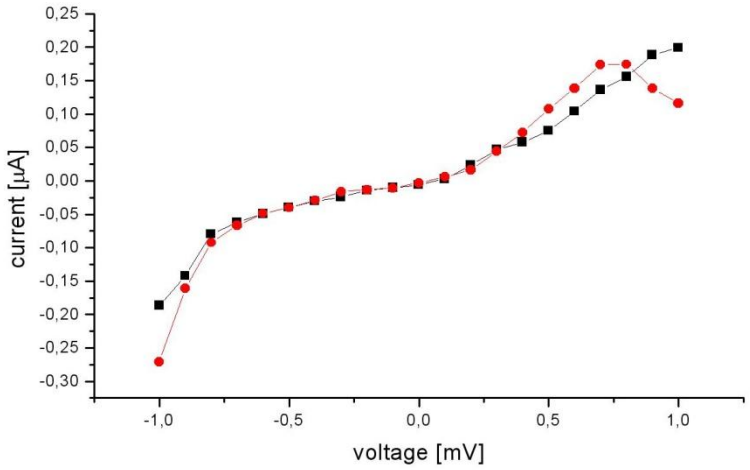

figure 9: Spectroscopy of the graphite sample (I (U); 50x 50Å; gapvoltagerange: -1 to 1V with a stepsize of 0,1V; 1540µs); red points: hightened position; black squares a lower position

2.3. 100nm Boron Doped Diamond Thin Film Sample

The following measurements and micrographs were taken from a 100nm boron doped diamond thin film sample (06309-I) which was deposited on a silicon single crystal substrate. The sample consists of different layers: a silicon bottom with a 1000nm silica layer on it and above this silica layer there are 4nm of titanium.

This sample was firstly analyzed with varying scanning parameters and experimental set ups in order to determine the optimal values.
The results of this analysis are:

I. The lamellar structure on the surface should be straightened in a 90 degree angle to the scan direction (namely 90 degrees to the measured lines of the scan). Because of fortune all samples were already straightened in the optimal direction for the scans. But the scanning angle could be adjusted for the microscope. Varying this angle led to measurements with lower qualities.

II. It is very important to turn off any disturbing devices during the scans in order to achieve proper images. Devices creating electromagnetic fields, in fact, almost any electric device could affect the measurements. Also vibrations may have effects on the scans. These negative influences mainly count at very high resolutions and have only very little influence on scans at a size of e.g. 5000Å.

III. For some scanning times the resulting data has a superposed oscillating part which distorts the image. To solve this problem one has to change the scanning time. It is important not to choose a multiple of the supply frequency which would again lead to oscillations.

A very good graphical tool to demonstrate the surface structure is also a profile graph. The next figure shows an exemplarily profile of a 5000 times 5000Å scan.

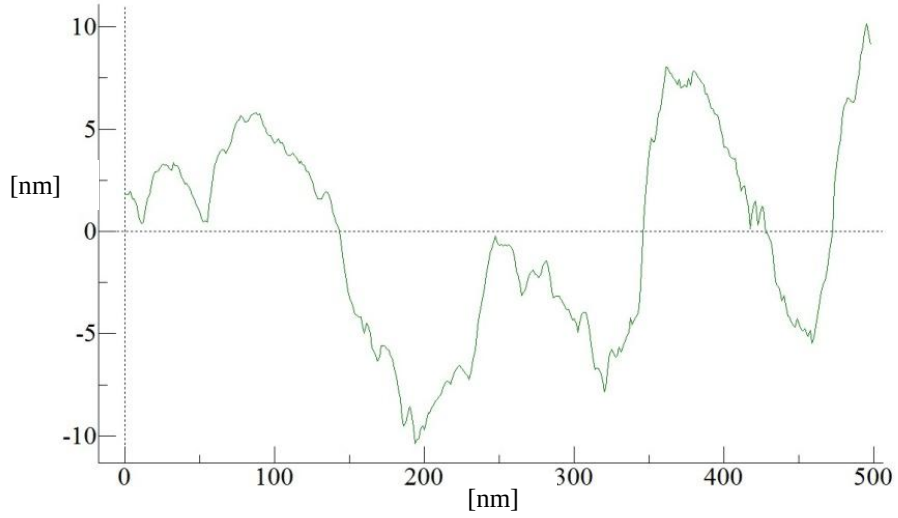

figure 10: Profile of the 100nm layer surface (x- direction: position on surface [nm], y- direction: height [nm]; the graph is centered at the average height of the surface)

One can see that the distances between the irregularities have nearly the same scale which is about 150nm. The maximum height measured from the lowest to the highest point of the surface is 30nm. As can be seen in the profile graph above and also in the following micrographs there is also a smaller lamellar structure within the big main structure. It is very hard to measure the scale of those small structures because they differ a lot across even one single 5000 x 5000Å scan. But they seem to lie in an area between 2 to 4nm.
The following figure 11 shows a compound of six displaced micrographs arranged together. The x- and y- direction offset can be set on the STM control unit. The resulting image of this sample has a size of 1000 x 700 nm.

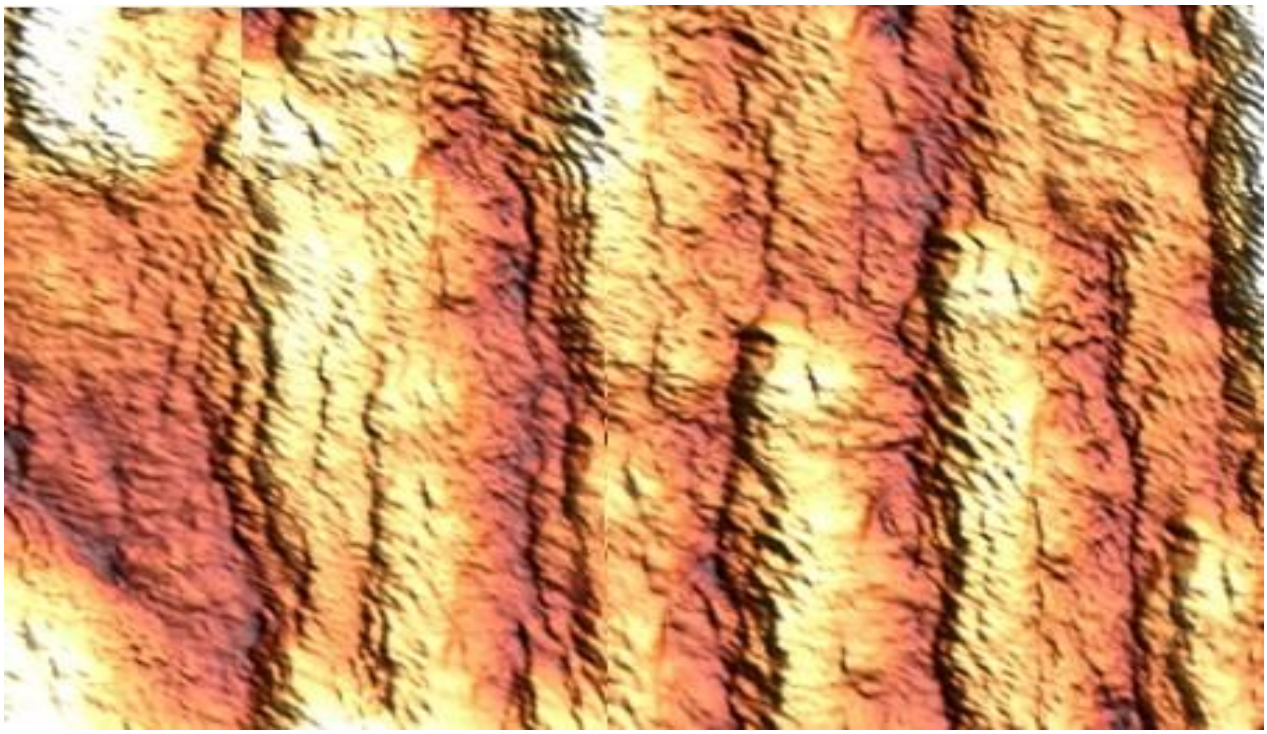

figure 11: Overview scan of the 100nm sample (1000 x 700nm; 3V; 0,1nA)

This figure shows a relief with a scaly lamellar structure which looks like an alternating formation of valleys and ridges. Within this main structure there is a smaller, more irregular, but similar structure of alternating ridges.
The average height of the irregularities of the 100nm layer is 130Å. The height above the average is 165Å which is 30% of the overall layer thickness. Figure 12 shows the height distribution of the sample in a bar chart in a presentable way:

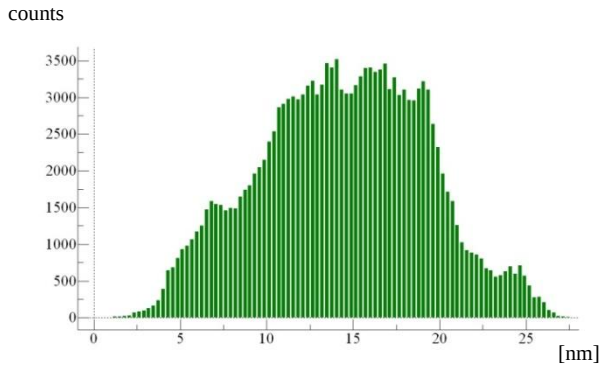

figure 12: Height distribution 100nm sample
(x- axis: height in nm; y- axis: counts)

In the following figures 13 to 16 one can see more detailed scans of the ridge in the left upper part of figure 11. They have a range from 2000Å down to 100Å.

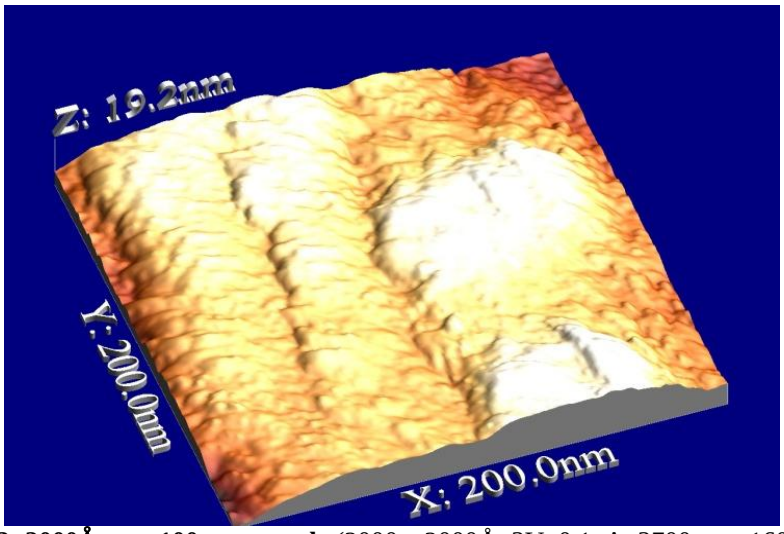

figure 13: 2000Å scan 100 nm sample (2000 x 2000Å; 3V; 0,1nA; 3700µs at 1600 steps)

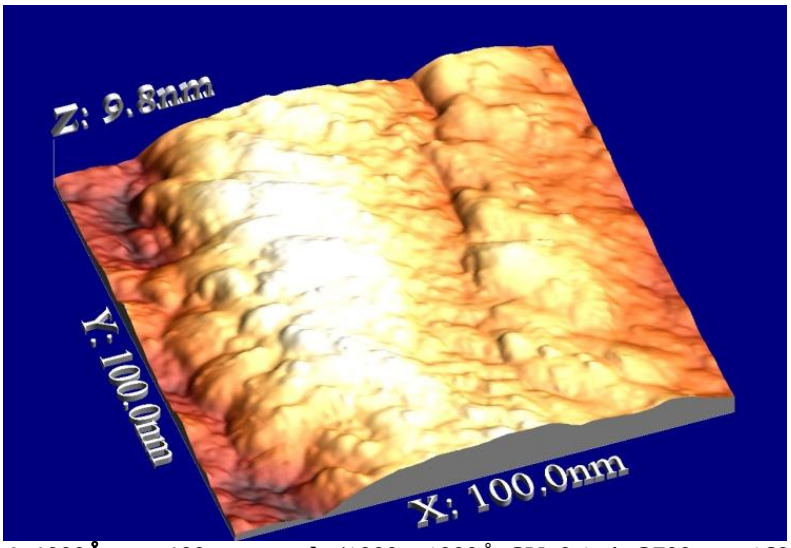

figure 14: 1000Å scan 100nm sample (1000 x 1000Å; 3V; 0,1nA; 3700µs at 1600 steps)

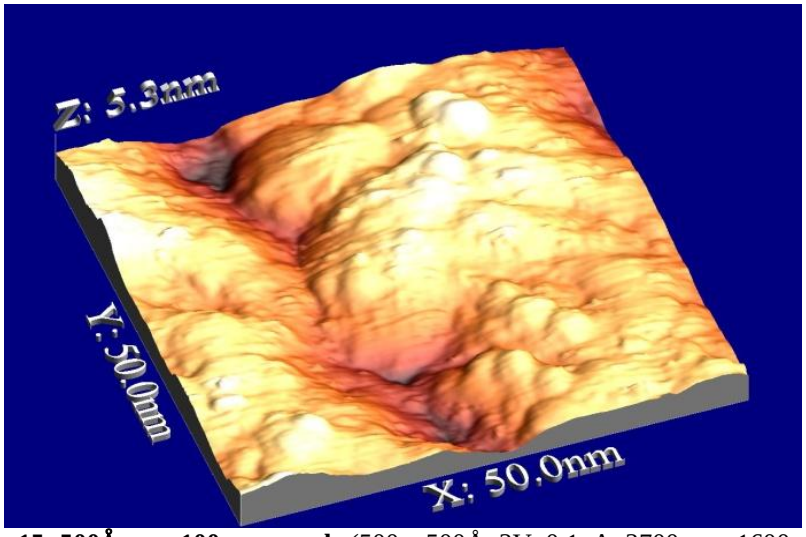

figure 15: 500Å scan 100nm sample (500 x 500Å; 3V; 0,1nA; 3700µs at 1600 steps)

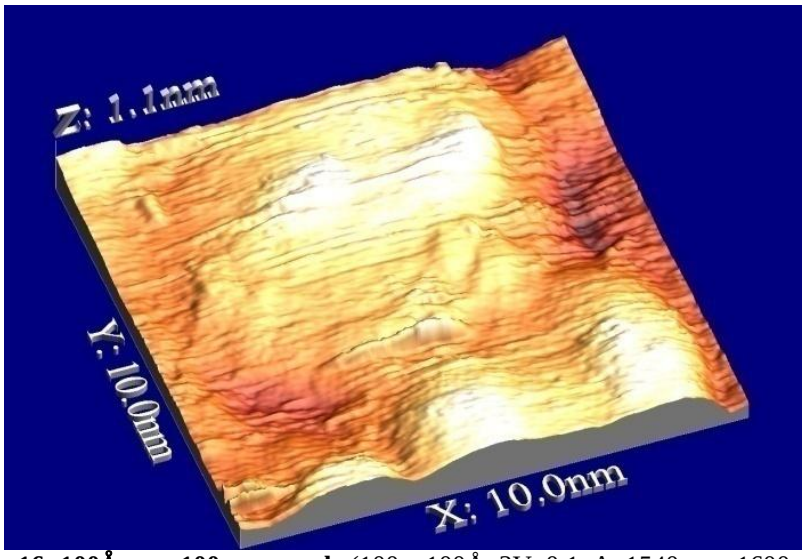

figure 16: 100Å scan 100nm sample (100 x 100Å; 3V; 0,1nA; 1540µs at 1600 steps)

Figure 16 shows that scans below 200 x 200Å do not contain any additional information. In fact the micrograph shows up lines distorting the image.

Figures 17 and 18 show high resolution scans of a deep valley:

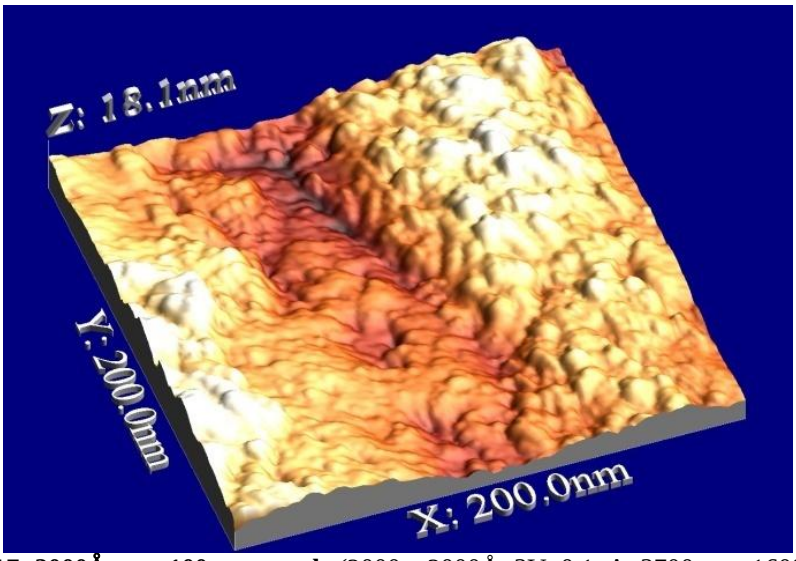

figure 17: 2000Å scan 100nm sample (2000 x 2000Å; 3V; 0,1nA; 3700µs at 1600 steps)

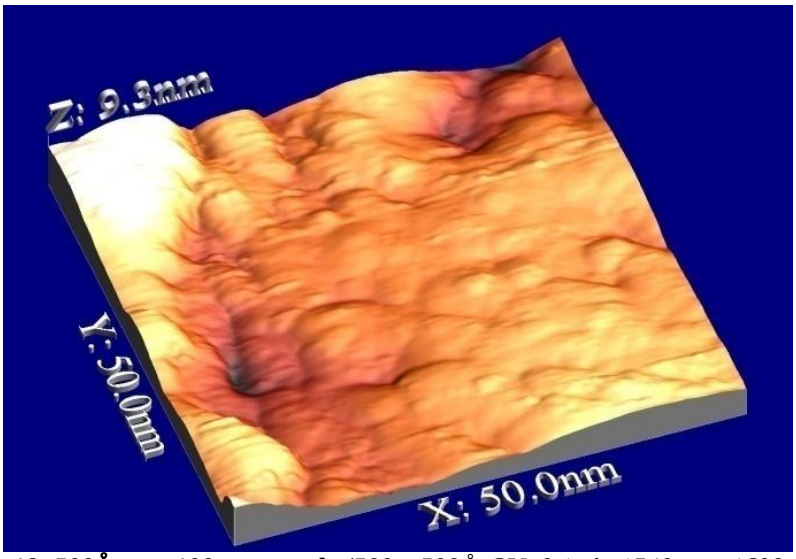

figure 18: 500Å scan 100nm sample (500 x 500Å; 3V; 0,1nA; 1540µs at 1600 steps)

A spectroscopic analysis gives information about the occupied and unoccupied states of the sample material. The measurements show that the boron doped diamond sample is conductive but has semiconductor characteristics. The figures 19 and 20 show a spectroscopic analysis of a ridge and a valley respectively:

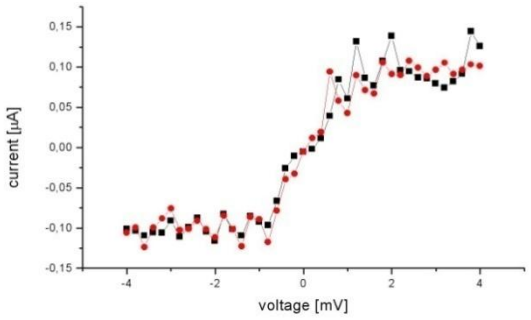

figure 19: Spectroscopy of 100nm sample (ridge) (I (U); 500x 500Å; gapvoltagerange: -1 to 1V with a stepsize of 0,1V; 1540µs); red points: hightened position; black squares a lower position

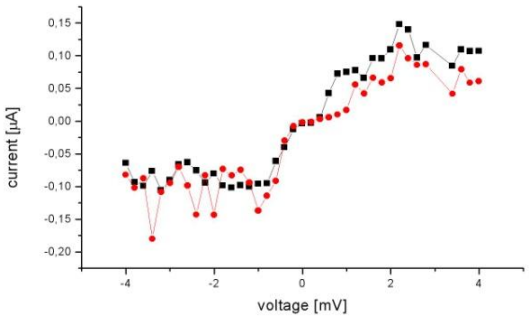

figure 20: Spectroscopy of 100nm sample (valley) (I (U); 500x 500Å; gapvoltagerange: -1 to 1V with a stepsize of 0,1V; 1540µs); red points: hightened position; black squares a lower position

2.4. 200nm Boron Doped Diamond Thin Film Sample

The following measurements and micrographs were taken from a 200nm boron doped diamond thin film sample (311008- III). The substrate on which the diamond layer was coated on has the same configuration as the 100nm sample (Si/ 100nm SiO_2/ 4nm Ti).

Figure 21 is a large area scan with an overall size of 1300 x 900nm. It consists of six single overlapping scans arranged together.

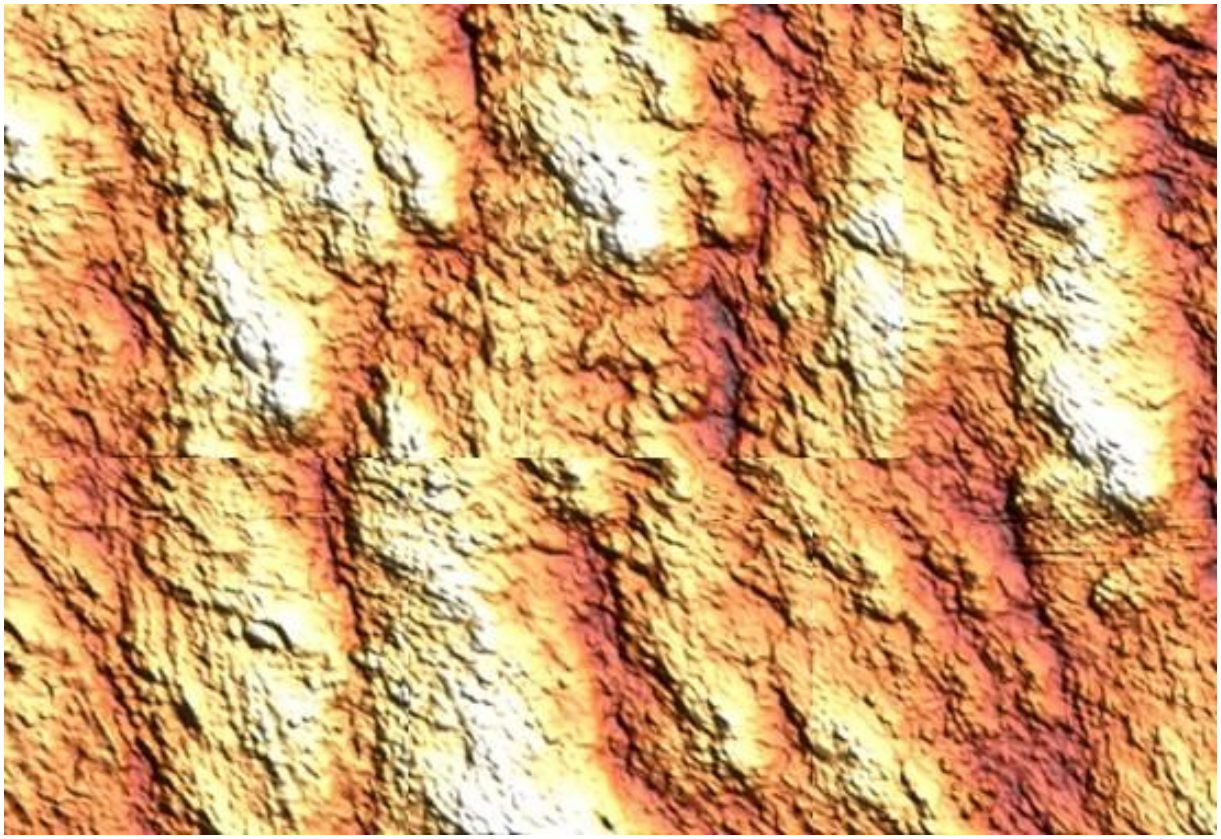

figure 21: Assembled picture of the 200nm sample (1300 x 900nm; 3V; 0,1nA)

The scan also shows a scaly lamellar structure, but it is not as pronounced compared to the 100nm sample. The surface also shows by far lower ceilinged elevations which make the sample look more irregular than the sample before.

The figures 22 to 24 show a series of detailed topographic images of a high ridge, with an imaged area from 2000 x 2000Å to 500 x 500Å:

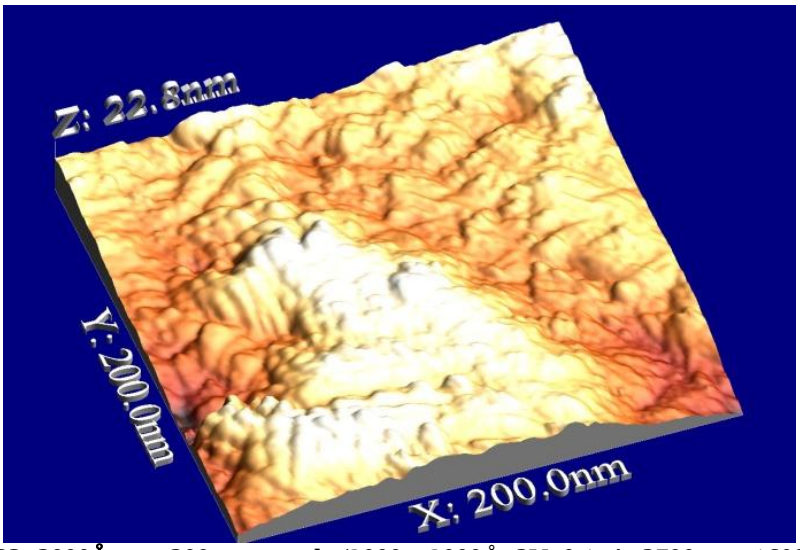

figure 22: 2000Å scan 200nm sample (2000 x 2000Å; 3V; 0,1nA; 3700µs at 1600 steps)

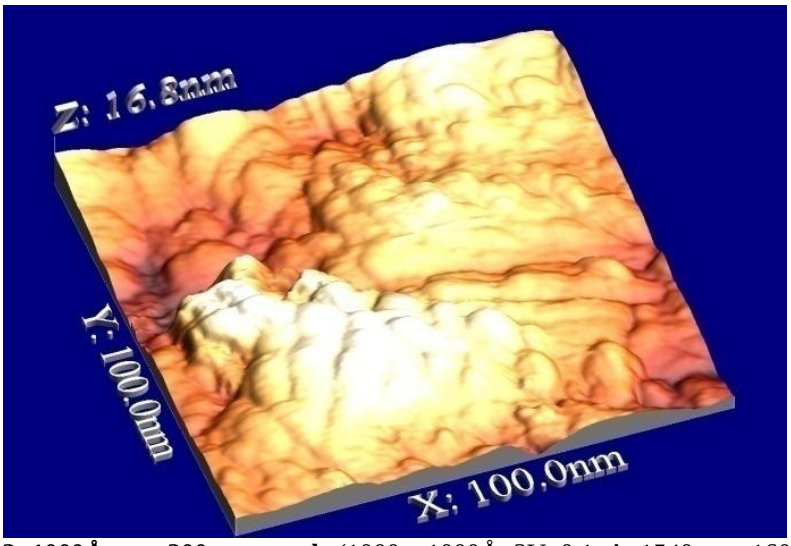

figure 23: 1000Å scan 200nm sample (1000 x 1000Å; 3V; 0,1nA; 1540µs at 1600 steps)

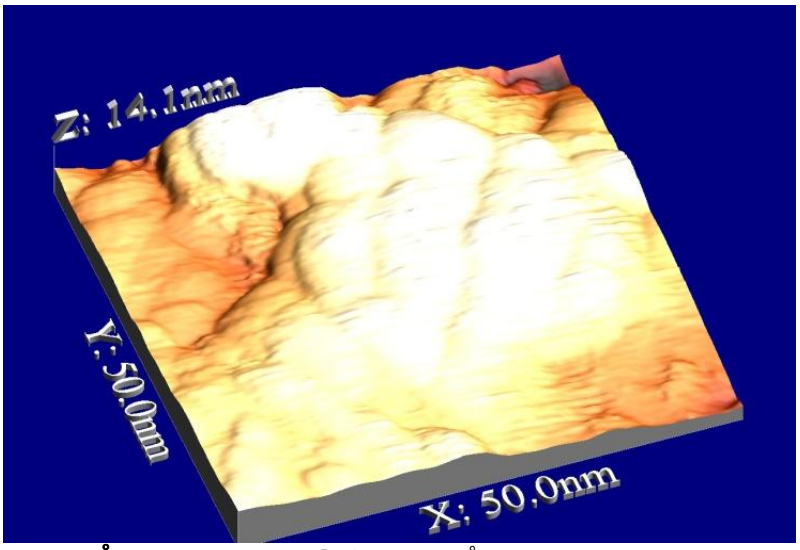

figure 24: 500Å scan 200nm sample (500 x 500Å; 3V; 0,1nA; 1540µs at 1600 steps)

The figures 25 to 28 show a series of detailed topographic images of a deep valley, with an imaged area from 2000 x 2000Å to 500 x 500Å:

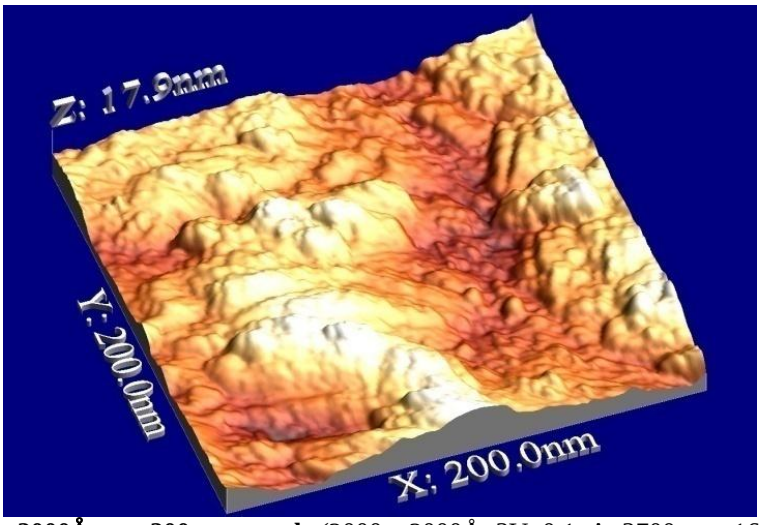

figure 25: 2000Å scan 200nm sample (2000 x 2000Å; 3V; 0,1nA; 3700µs at 1600 steps)

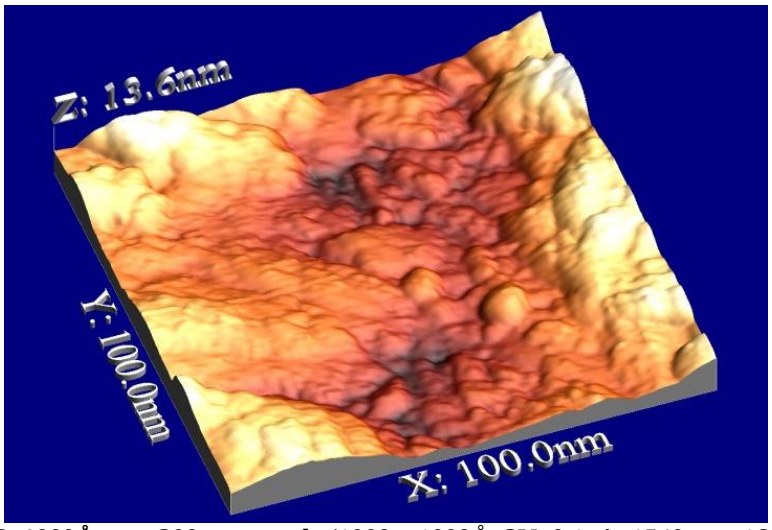

figure 26: 1000Å scan 200nm sample (1000 x 1000Å; 3V; 0,1nA; 1540µs at 1600 steps)

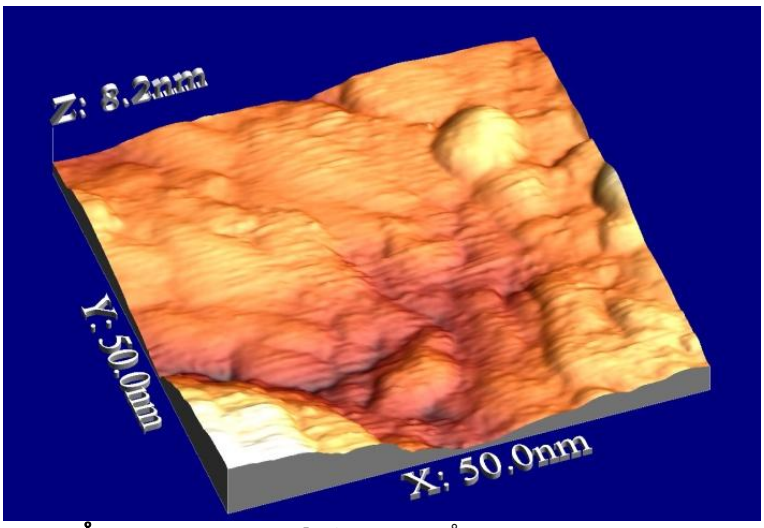

figure 27: 500Å scan 200nm sample (500 x 500Å; 3V; 0,1nA; 1540µs at 1600 steps)

Figure 28 is a profile graph of the 200nm diamond layer of an area of 5000 x 5000Å:

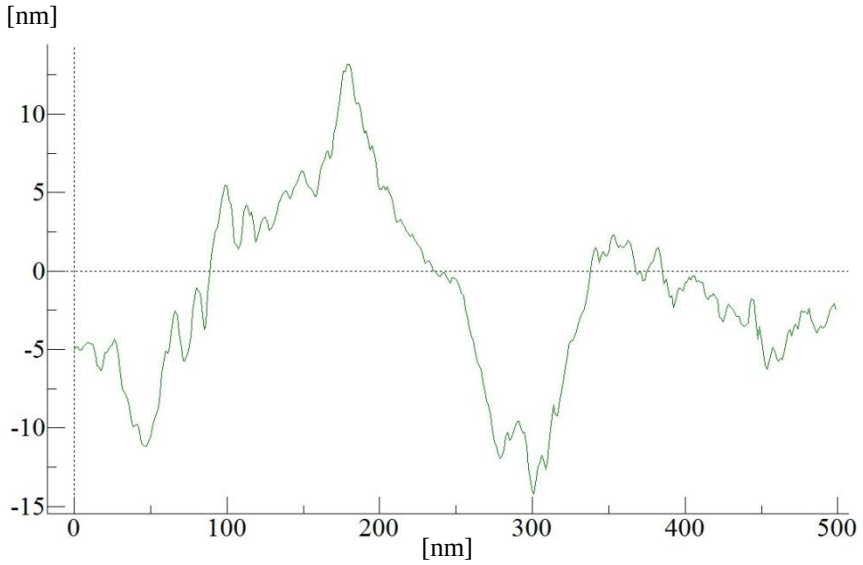

figure 28: Profile of the 200nm layer surface (x- direction: position on surface [nm], y- direction: height [nm]; the graph is centered at the average height of the surface)

One can see that the distances between the irregularities have nearly the same scale which is about 250nm. The maximum height measured from the lowest to the highest point of the surface is 31nm. As can be seen in the profile graph above and also the other micrographs there is also a smaller lamellar structure within the big main structure, although it is not as pronounced as on the surface of the 100nm thick layer. The height of the small lamellas is about 3nm. Figure 29 shows the height distribution in a bar chart:

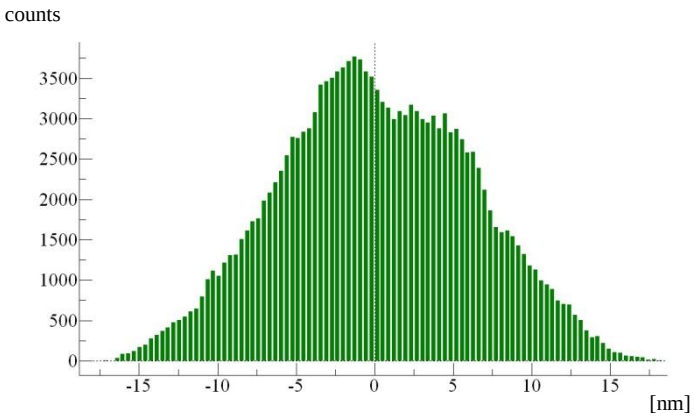

figure 29: Height distribution 200nm sample
(x- axis: height in nm; y- axis: counts)

The average height of the irregularities of the 100nm layer is 140Å. The height above the average is 165Å which is 15% of the overall layer thickness.

A spectroscopic scan shows nearly the same properties as the measurements on the 100nm layer sample. The measurements were taken on a 200 x 200Å area; figures 29 and 30 show the results:

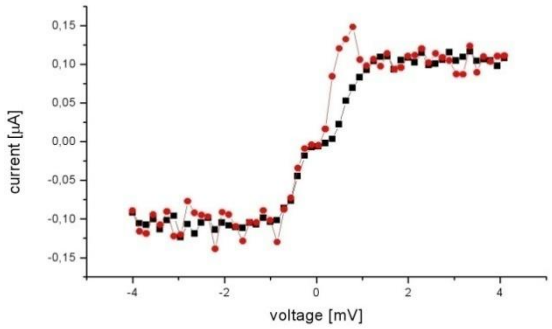

figure 30: Spectroscopy of 200nm sample (ridge) (I (U); 500x 500Å; gapvoltagerange: -1 to 1V with a stepsize of 0,1V; 1540µs)

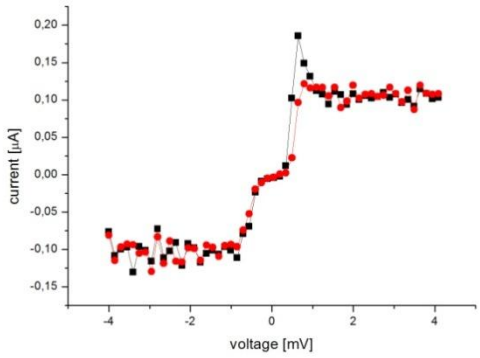

figure 31: Spectroscopy of 200nm sample (valley) (I (U); 500x 500Å; gapvoltagerange: -1 to 1V with a stepsize of 0,1V; 1540µs)

2.5. 500nm Boron Doped Diamond Thin Film Sample

The following measurements and micrographs were taken from a 500nm boron doped diamond thin film sample (060309- II). The substrate on which the diamond layer was coated on has the same configuration as the 100nm sample (Si/ 100nm SiO_2/ 4nm Ti).

Figure 32 is a large area scan with an overall size of 1400 x 900nm. It consists of six single overlapping scans arranged together.

figure 32: Assembled picture of the 500nm sample (1400 x 900nm; 3V; 0,1nA)

Like in the other samples the 500nm specimen shows the lamellar structure but with far broader ridges but also greater height differences. The smaller lamellar structure on the other hand is less regular and is even less pronounced than on the 200nm thick layer sample.

The figures 33 to 35 show a series of detailed topographic images of a high ridge, with an imaged area from 2000 x 2000Å to 500 x 500Å:

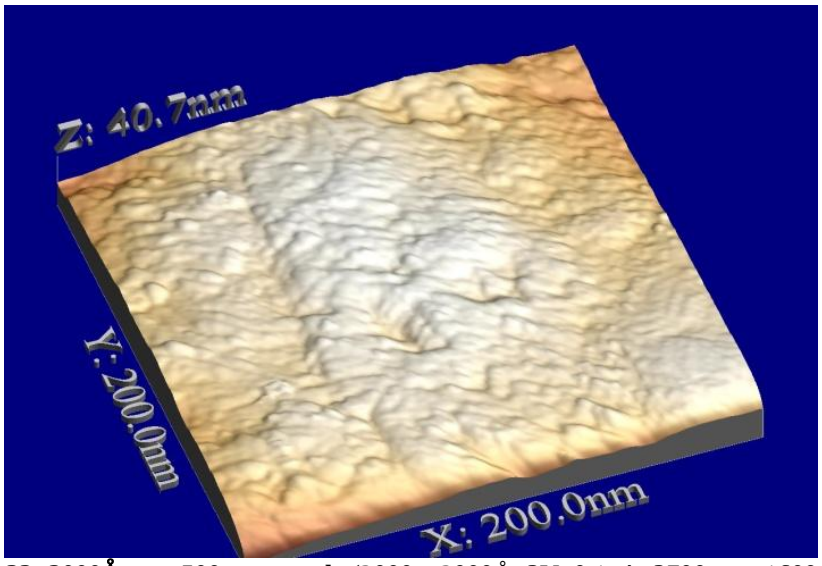

figure 33: 2000Å scan 500nm sample (2000 x 2000Å; 3V; 0,1nA; 3700µs at 1600 steps)

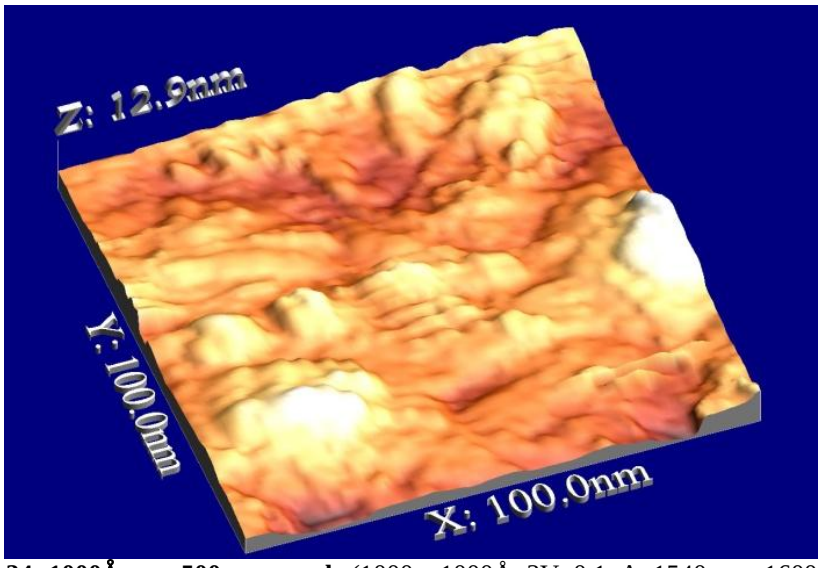

figure 34: 1000Å scan 500nm sample (1000 x 1000Å; 3V; 0,1nA; 1540µs at 1600 steps)

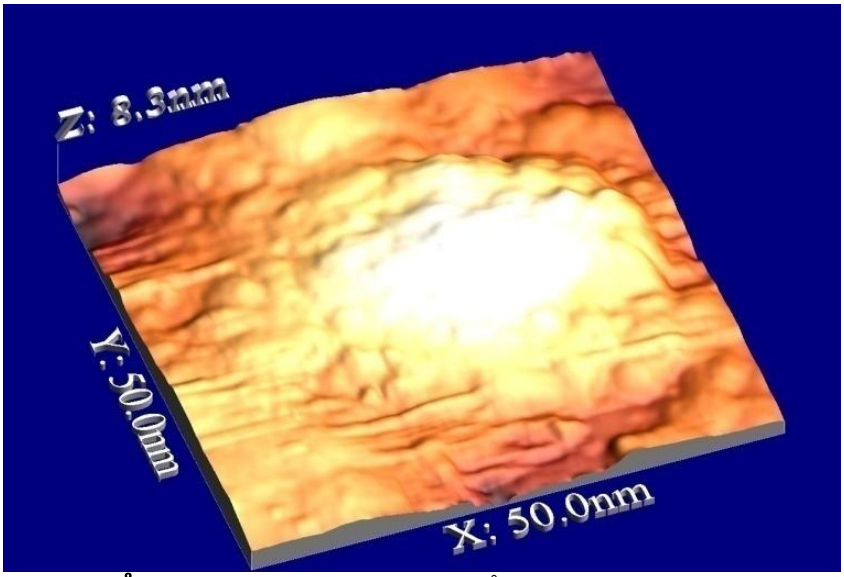

figure 35: 500Å scan 500nm sample (500 x 500Å; 3V; 0,1nA; 1540µs at 1600 steps)

The figures 36 to 38 show a series of detailed topographic images of a deep valley, with an imaged area from 2000 x 2000Å to 500 x 500Å:

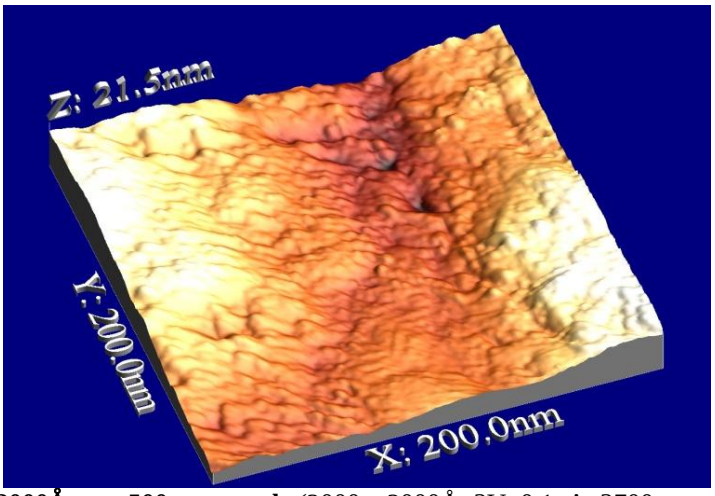

figure 36: 2000Å scan 500nm sample (2000 x 2000Å; 3V; 0,1nA; 3700µs at 1600 steps)

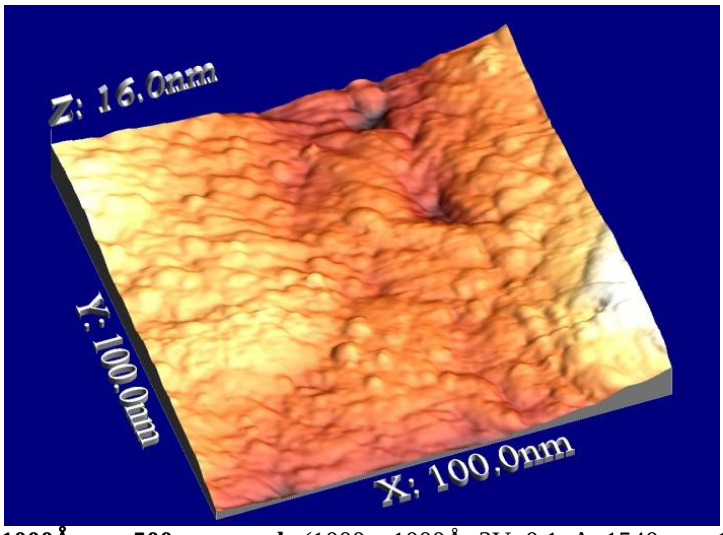

figure 37: 1000Å scan 500nm sample (1000 x 1000Å; 3V; 0,1nA; 1540µs at 1600 steps)

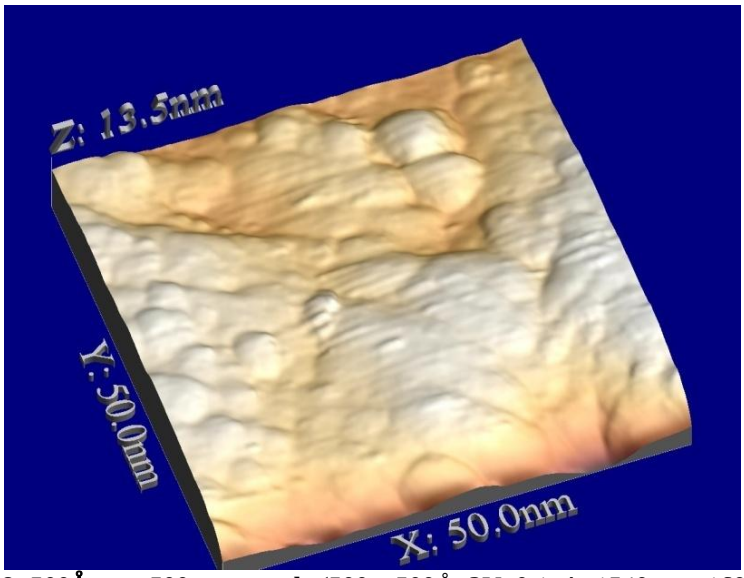

figure 38: 500Å scan 500nm sample (500 x 500Å; 3V; 0,1nA; 1540µs at 1600 steps)

Figure 39 is a profile graph of the 500nm diamond layer of an area of 5000 x 5000Å:

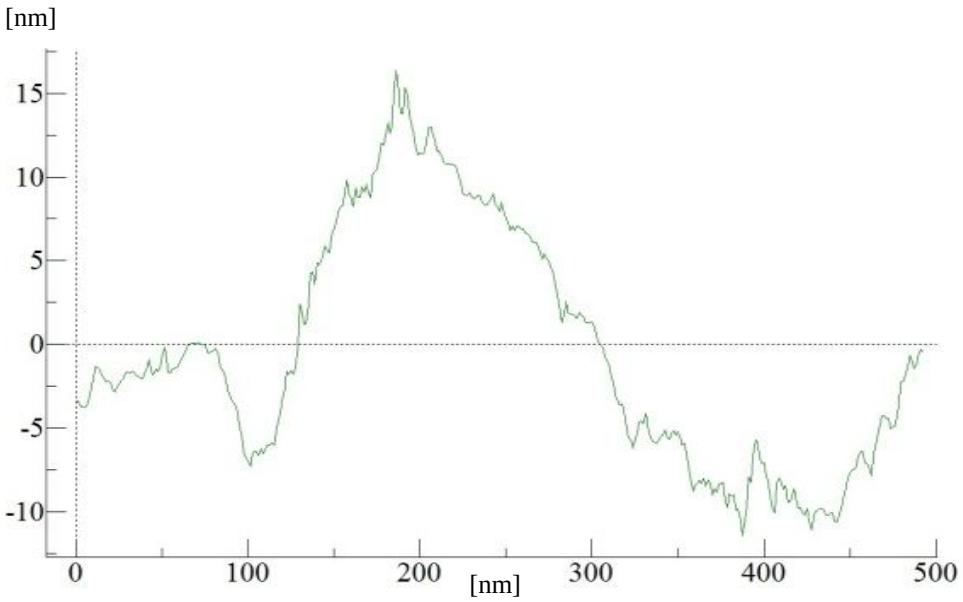

figure 39: Profile of the 500nm layer surface
(x- direction: position on surface [nm], y- direction: height [nm]; the graph is centered at the average height of the surface)

One can see that the distances between the irregularities have a larger scale which is about 400nm. The maximum height measured from the lowest to the highest point of the surface is 47nm. The mean height of the smaller lamellas is about 10nm but by far not as pronounced compared to the thinner specimen. Figure 40 shows the height distribution in a bar chart:

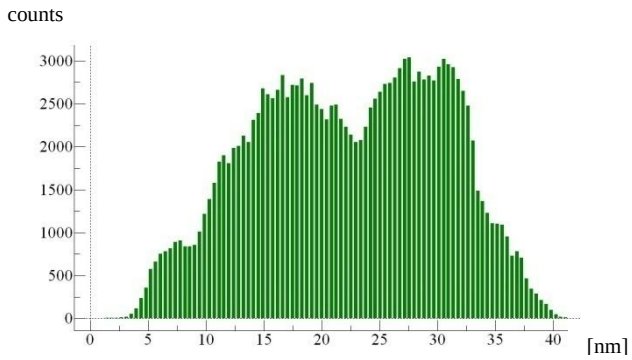

figure 40: Height distribution 500nm sample
(x- axis: height in nm; y- axis: counts)

The average height of the irregularities of the 500nm layer is 225Å. The height above the average is 240Å which is 9% of the overall layer thickness. Compared to the thinner layers the 500nm layer has no distinct height distribution maximum. It has a local minimum at the centre of the distribution and below and above a maximum.

A spectroscopic scan shows nearly the same properties as the measurements on the 100nm and 200nm layer sample. The measurements were taken on a 200 x 200Å area; figures 41 and 42 show the results:

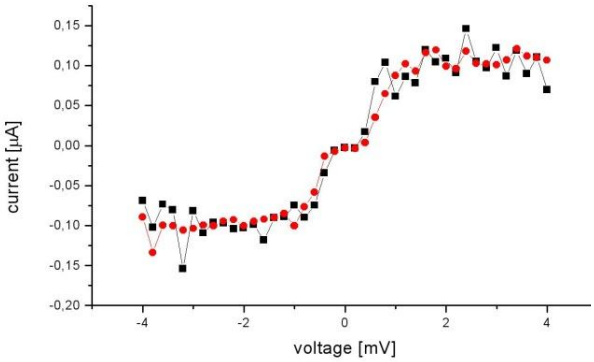

figure 41: Spectroscopy of 500nm sample (ridge) red points: hightened position; black squares a lower position

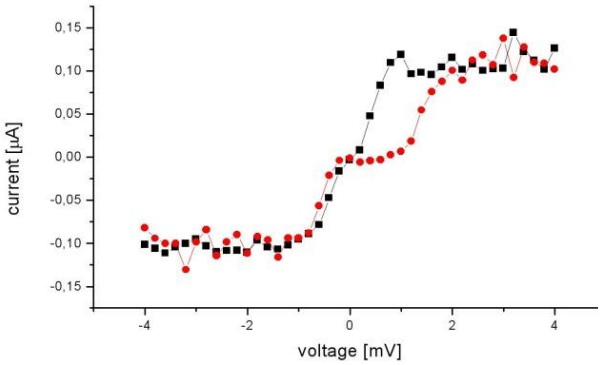

figure 42: Spectroscopy of 500nm sample (valley) red points: hightened position; black squares a lower position

2.6. 500nm Undoped Diamond Thin Film Sample

The following measurements and micrographs were taken from a 500nm undoped diamond thin film sample. The substrate on which the diamond layer was coated on has the same configuration as the other samples (Si/ 100nm SiO_2/ 4nm Ti).

Figure 43 is a large area scan with an overall size of 1100 x 900nm. It consists of six single overlapping scans arranged together.

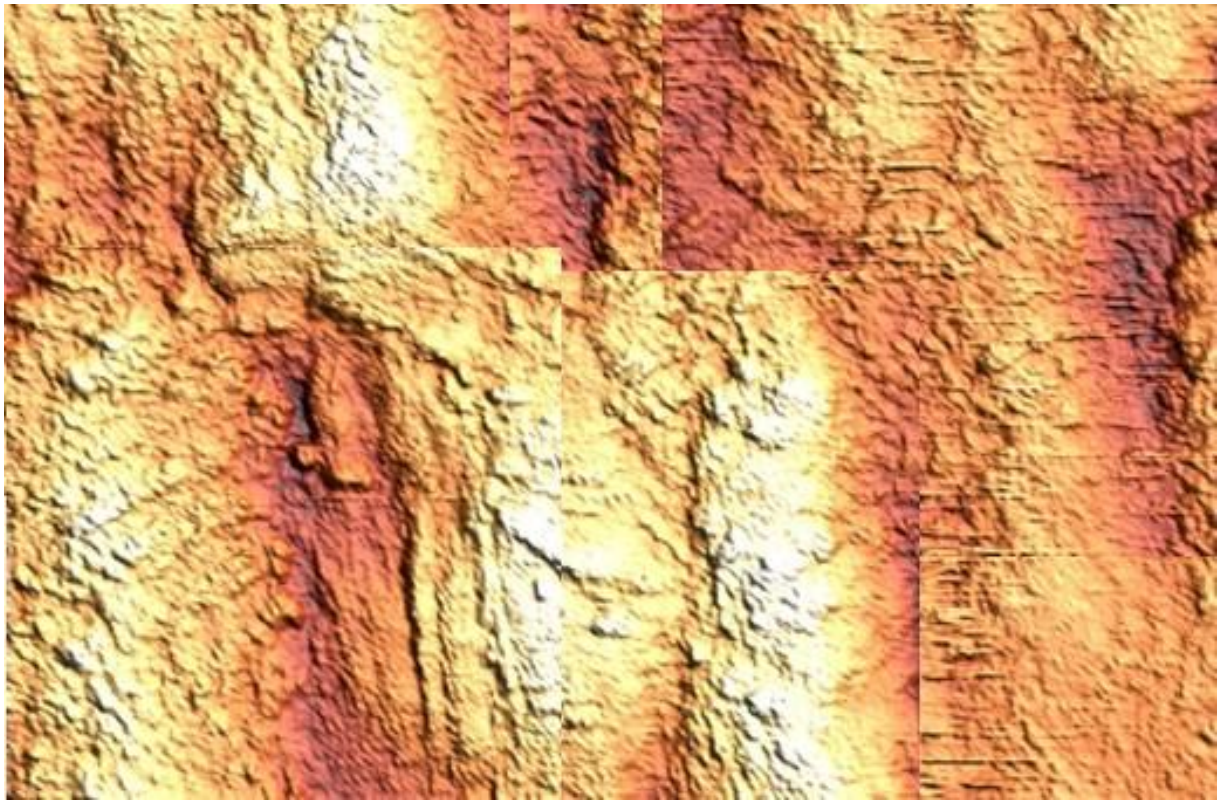

figure 43: Assembled picture of the 500nm undoped sample

Like in the other samples the 500nm undoped layer specimen shows the same lamellar structure like the 500nm doped diamond layer sample.

The figures 44 and 45 show two detailed topographic images of a high ridge, with an imaged area from 1000 x 1000Å and 500 x 500Å:

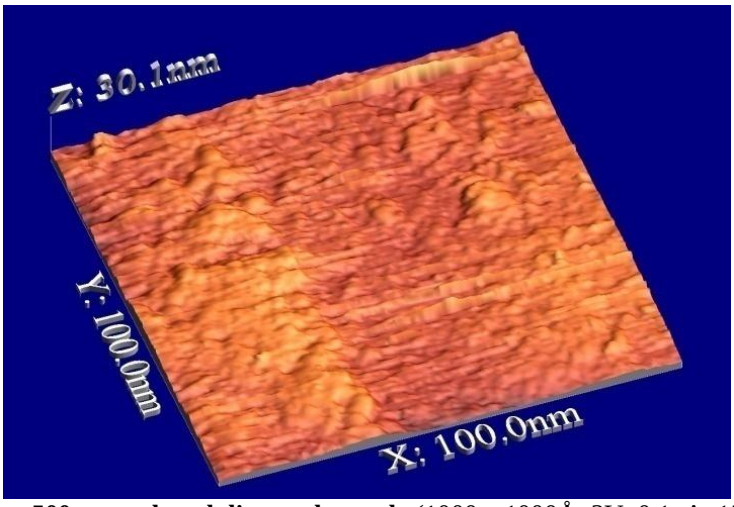

figure 44: 1000Å scan 500nm undoped diamond sample (1000 x 1000Å; 3V; 0,1nA; 1540µs at 1600 steps)

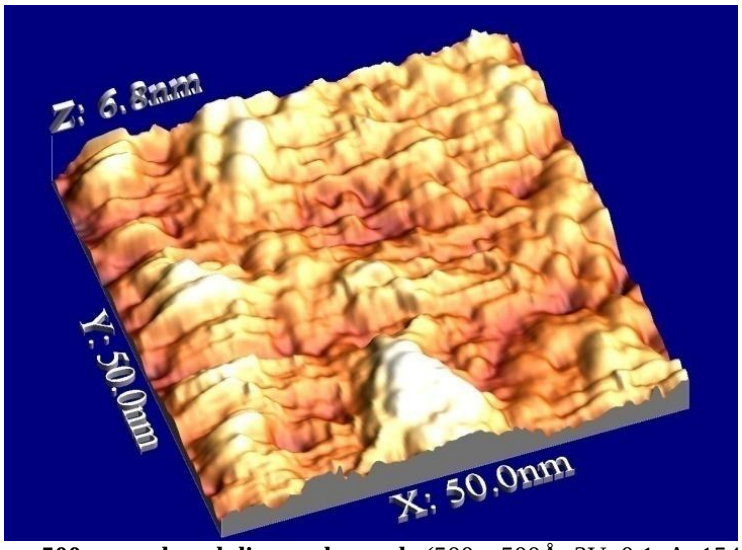

figure 45: 500Å scan 500nm undoped diamond sample (500 x 500Å; 3V; 0,1nA; 1540µs at 1600 steps)

The figures 46 and 47 show two detailed topographic images of a deep valley, with an imaged area of 2000 x 2000Å and 1000 x 1000Å:

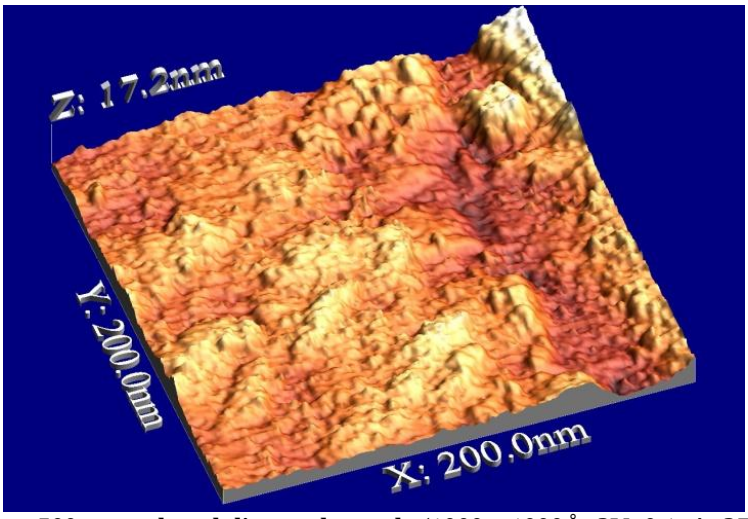

figure 46: 2000Å scan 500nm undoped diamond sample (1000 x 1000Å; 3V; 0,1nA; 3700µs at 1600 steps)

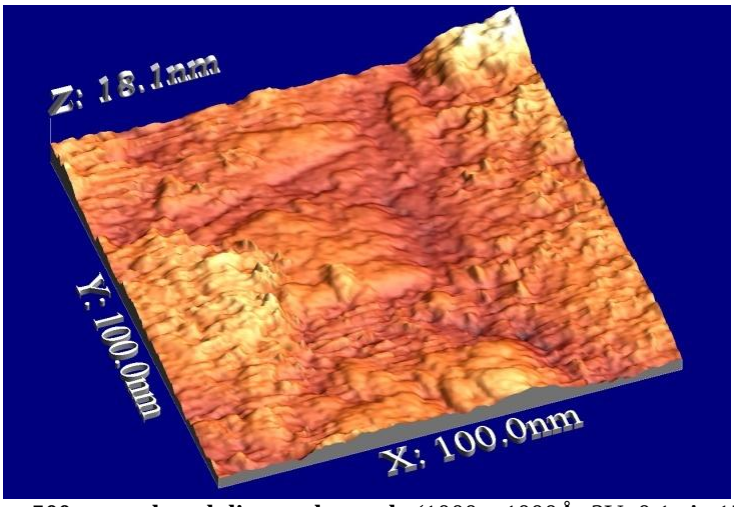

figure 47: 1000Å scan 500nm undoped diamond sample (1000 x 1000Å; 3V; 0,1nA; 1540µs at 1600 steps)

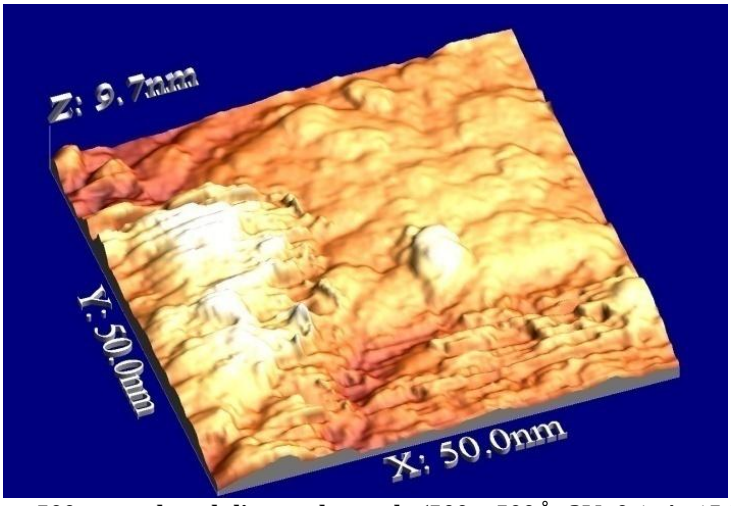

figure 48: 500Å scan 500nm undoped diamond sample (500 x 500Å; 3V; 0,1nA; 1540µs at 1600 steps)

Figure 49 is a profile graph of the 500nm undoped diamond layer of an area of 5000 x 5000Å:

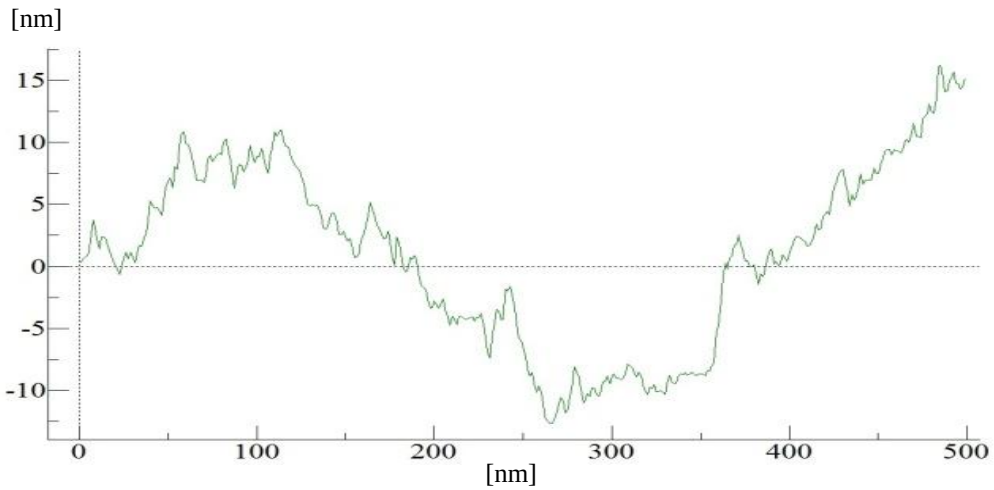

figure 49: **Profile of the 500nm undoped layer surface** (x- direction: position on surface [nm], y- direction: height [nm]; the graph is centered at the average height of the surface)

One can see that the distances between the irregularities have quite the same scale which is about 400Å. The maximum height measured from the lowest to the highest point of the surface is 390Å and the mean height of the smaller lamellas is about 10nm. Figure 50 shows the height distribution in a bar chart:

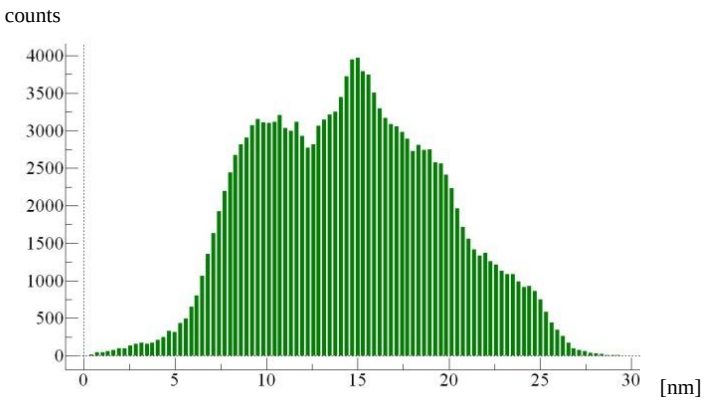

figure 50: Height distribution 500nm undoped sample (x- axis: height in nm; y- axis: counts)

The average height of the irregularities of the 500nm undoped diamond layer is 160Å. The height above the average is 230Å which is 8% of the overall layer thickness. Compared to the thinner layers the 500nm layer has no distinct height distribution maximum like the 500nm doped diamond layer sample.

A spectroscopic scan shows nearly the same properties as the measurements on the 100nm and 200nm layer sample. The measurements were taken on a 200 x 200Å area; figures 51 and 52 show the results:

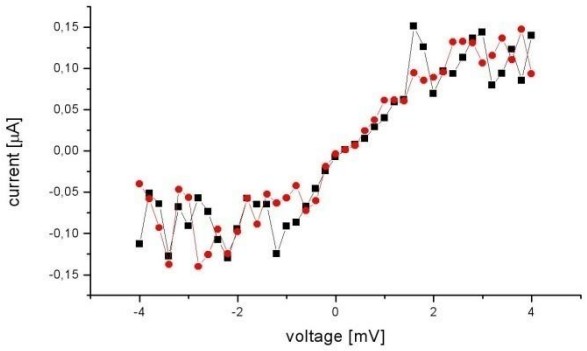

figure 51: Spectroscopy of 500nm undoped sample (ridge) red points: hightened position; black squares a lower position

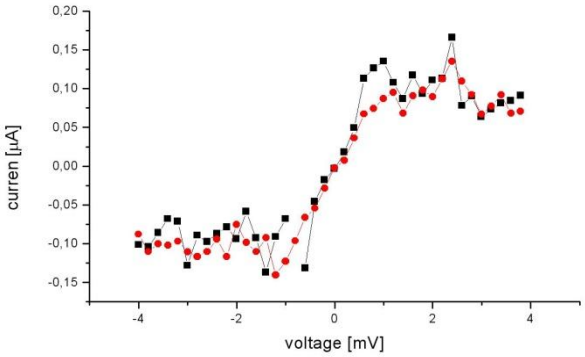

figure 52: Spectroscopy of 500nm undoped sample (valley) red points: hightened position; black squares a lower position

The figures proof what could be estimated already before the measurements: it is much more difficult to get a good scan without aberrations of the pure diamond layer. The reason for that is the semiconductor characteristic of the diamond structure. Carbon arranged in the diamond structure is not conductive, but, because of diffused titanium atoms, measurements are practicable though.

3. Conclusion

The task of this thesis was to observe the surface structures of diamond coated silicon samples and in the following to make a statement about the growing process. Each of the measured samples had a different thickness of the diamond layer which was brought onto the specimen by plasma vapor deposition. The diamond layers differed in thickness and doping. Overall the surface structures do not differ much comparing the 4 different samples. The surfaces show some kind of macro- and within again another micro- lamellar, scaly structure but the structures have different dimensions and vary in their distinction. The distances between the micro lamellas cannot be measured clearly because they are distributed very irregular. The 100nm diamond coated sample has a gap between the ridges of the surface at the size of 150nm and a maximum height aberration of 30nm. Although the distance between the lamellas of the 200nm diamond coated sample is increased to 250nm the overall differences to the 100nm sample is nearly negligible. The 500nm boron doped layer and the 500nm undoped layer sample also show very few differences in their structures. But of course the spectroscopic scans show higher differences. The distance between their lamellas is 400nm and their maximum height aberration lies at about 10% percent of the layer thickness. This structures lead to the suggestion that the growth of the diamond layers using plasma vapor deposition is a combined layer and island growth. What means that the growth is not uniform and that the layer has preferred areas of growth. It can be said that the film thickness has low influences on the structure, besides that the size of the aberrations increases with the layer thickness and that the distinction of the micro lamellar structure decreases and becomes more irregular.

The spectroscopic scans show the probability of electrons to tunnel at a certain voltage. So the levels can be shown which contribute to the conductivity of the different samples. All boron doped samples show conductivity in principal but also a pronounced semiconductor characteristic. On the other hand the undoped diamond layer sample shows a by far increased semiconductor characteristic. The relatively high probability for the electrons to tunnel at a certain voltage can probably explained by diffusing titanium atoms.

In conclusion, it can be said that the diamond thin films have an increasing roughness in their surface structure with increasing layer thickness. The doping of the carbon has no effect on the surface structure, but of course on the electronic properties. Apparently the observation of the several samples shows that plasma vapor deposition initiates a combined layer by layer and island growth.

4. References

1. H. G. Evertz, W. von der Linden. Skriptum Quantenmechanik (3. Auflage). 89- 128. (2007).
2. R. M. Dreizler, C. S. Lüdde. Theoretische Physik Band 3: Quantenmechanik 1. 87-139. (2008).
3. H. J. Güntherodt, R.Wiesendanger. Scanning Tunneling Microscopy I. 1- 10. (1996).
4. E. Meyer, H. J. Hug, R Bennewitz. Scanning Probe Microscopy. The Lab on a Tip. 2-10. (2003).
5. A. Krüger. Neue Kohlenstoffmaterialien. Eine Einführung. (1. Auflage). 1- 10. (2007).
6. Nanotec Elctronica. WSxM 5.0 Develop 1.2